



Article

Integrated WPT-PLC System Applied to UAV: Characterization of a Two-Coil Channel Considering Misalignment Scenarios

Safa Zouaoui ^{1,2}, Wael Dghais ^{1,2,3} , Luis Romba ⁴, Rui Melicio ^{5,6,*}  and Hamdi Belgacem ^{1,2,3}

- ¹ Faculté des Sciences de Monastir, Université de Monastir, Monastir 5000, Tunisia; saf_a_zouaoui@yahoo.com (S.Z.); waeldghais@ua.pt (W.D.); belgacem.hamdi@gmail.com (H.B.)
- ² Laboratoire d'Electroniques et Microélectroniques, Université de Monastir, Monastir 5000, Tunisia
- ³ Institut Supérieur des Sciences Appliquées et de Technologie de Sousse, Université de Sousse, Sousse 4003, Tunisia
- ⁴ Centre of Technology and Systems, Faculdade de Ciências e Tecnologia, Universidade NOVA de Lisboa, 2829-516 Monte Caparica, Portugal; romba.jorge@gmail.com
- ⁵ Mechanical Engineering Institute (IDMEC), Instituto Superior Técnico, Universidade de Lisboa, Av. Rovisco Pais 1, 1049-001 Lisboa, Portugal
- ⁶ Instituto de Ciências da Terra (ICT), Universidade de Évora, Rua Romão Ramalho, 59, 7002-554 Évora, Portugal
- * Correspondence: ruimelicio@gmail.com; Tel.: +35-121-841-7351

Abstract: WPT system performances highly depend on the misalignment scenarios of the transmitter or the receiver coil. In this contribution, the authors analyze the effect of the misalignment influencing factors of the integrated WPT-PLC system receiving coil on the system performances. The simulations and experimental analysis are based on power efficiency and channel capacity metrics. The simulations are performed using finite element calculations in COMSOL Multiphysics and Advanced Design System (ADS) from Keysight technology. By analyzing the results, maximum transferred power is reached under resonance conditions. For instance, the calculated efficiencies versus the misalignment cases of the WPT-PLC system varies ($\eta = 86\%$ to 60%) when $d = [3 \text{ cm to } 7 \text{ cm}]$, $s = [3 \text{ cm to } 9 \text{ cm}]$, and for a tilt angle $\theta \leq 20 \text{ deg}$, while the optimal data rate $C(\text{bps})$ is achieved while appealing different data access points and under reasonable SNR value.

Keywords: wireless power transfer; inductive coupling; drones; UAV; data communication; bandwidth; data rate; misalignment; finite element simulation; multiphysics simulation



Citation: Zouaoui, S.; Dghais, W.; Romba, L.; Melicio, R.; Belgacem, H. Integrated WPT-PLC System Applied to UAV: Characterization of a Two-Coil Channel Considering Misalignment Scenarios. *Electronics* **2022**, *11*, 1249. <https://doi.org/10.3390/electronics11081249>

Academic Editor: Dimitra I. Kaklamani

Received: 25 January 2022

Accepted: 5 April 2022

Published: 15 April 2022

Publisher's Note: MDPI stays neutral with regard to jurisdictional claims in published maps and institutional affiliations.



Copyright: © 2022 by the authors. Licensee MDPI, Basel, Switzerland. This article is an open access article distributed under the terms and conditions of the Creative Commons Attribution (CC BY) license (<https://creativecommons.org/licenses/by/4.0/>).

1. Introduction

The use of air vehicles such as drones, UAVs, wing gliders, and aerostat airships have become increasingly popular in various applications, including aerial photography, product deliveries, agriculture, policing and surveillance, and infrastructure inspections, since the Federal Aviation Administration (FAA) issued the first commercial drone permit in 2006 [1,2]. Unfortunately, UAVs suffer from a decreased fly time due to fast battery drain, which limits their adoption in a 5G network. In addition, the restriction of existing solutions for communication and control between a drone and its controller becomes increasingly evident, especially with the expansion of drone applications [3,4]. The integration of WPT technology in air vehicles (AV) such as drones and UAVs with the concept of refueling/recharging a UAV during a mission can enable higher autonomy and mobility in such scenarios with fewer interruptions.

However, several authors have studied the possibility of integrating WPT technology in AV; the idea of refueling a UAV during a mission can provide the ability for longer missions and minimize human interaction [5–9]. In [5], the feasibility of the WPT charging system applied to the DJI F550 drone is performed and the magnetic field levels emitted by the WPT coil currents are analyzed while considering the misalignments between the coils. Moreover, with the aim of minimizing the misalignment effects and improving the landing

precision, in [6], the authors propose a new topology consisting of an array of independent coils used as a charging ground station, while in [7], this promising technology is integrated into a drone named Crazyflie 2.0 (Bitcraze AB, Malmö, Sweden) to wirelessly power a sensor network. Finally, in [8,9], the authors discuss the possibilities of using drones and UAVs for infrastructure inspections while proposing a dynamic wireless charging scenario considering the power lines as a source of the magnetic field.

In previous work [5–9], the receiver coil is mounted under the frame of the drone, with a vertical distance of at least 10 cm from the transmitter coil, causing a poor coupling coefficient, and in addition, the EM interference with the electronic components is already placed on the drone. However, in order to adopt this topology, additional turns in the secondary are required as well as considering the ferrite as a solution to achieve high WPT efficiency, which reduces the maximum weight of the pick-up. Moreover, the WPT systems previously discussed are considered for the UAV wireless charging medium while the data exchange is performed based on a supplementary communication module. However, the proposed system investigates the idea to share power and bidirectional data through the same channel; the new design requires the integration of decoupling filters, which can guarantee an effective separation between the power and data bandwidths while avoiding EM interferences, leading to a significant decrease in the weight of the integrated WPT solution, which guarantees a good compromise between complexity and system efficiency.

However, one of the major problems of the WPT technology applied to UAV technology is the poor landing precision, and the system's performances highly depend on the transmission distances and misalignment conditions of the secondary coil while considering a fixed transmitter coil. The contribution of this paper is to study the influence of the distances, the misalignment angle, and the horizontal deviation of the integrated WPT-PLC receiving coil on the system efficiency and also to calculate the channel capacity under various misalignment scenarios in order to assess the feasibility of simultaneous power and data transfer. The figure of merits characterizing the variability WPT-PLC link power and data conversion performance versus the separating distance and misalignment angle between the coupling coils (i.e., coupling factors) is presented by means of simulation in order to algorithmically and electrically optimize the proposed design and to consider these as the requirements while performing the experimental measurements in upcoming studies.

This paper is organized as follows. Section 2 describes the equivalent circuit model of the WPT system based on magnetically resonant coupling while considering the adequate decoupling filters. Section 3 optimizes the proposed architecture while integrating the power line technology. Sections 4 and 5 present and discuss the simulations and experimental results while introducing the possible misalignment scenarios. Finally, Section 6 discusses the findings.

2. Characterization of the Hybrid WPT-PLC System

Wireless power transfer with loosely coupled coils is a promising solution for delivering power to a battery in a variety of applications [10,11]. In such a system, the coil embedded in a receiving device picks up the energy transferred through the magnetic field induced by the transmitter coil; thus, contactless charging is achieved. With the aim of transmitting both power and data, adjacently but with separated frequency bands, the circuits shown in Figure 1 are analyzed and simulated within the COMSOL package. While considering the two-coil system, generally, the existing approaches use the same terminals of the power transfer as the data link [12], while in this contribution, different access points for the data terminals are performed in both systems. Firstly, the data modem is connected between the coils by avoiding the resonance capacitance C_1 and C_2 , respectively, as shown in Figure 1. The equivalent circuit of a magnetic integrated WPT-PLC two-coil system with a single TX coil and single RX coil can be easily represented as an equivalent circuit model based on lumped parameters (L_i, C_i, R_i) , where L_1, L_2 are the self-inductances of the 3D mutually coupled planar spiral coils. C_1 and C_2 are the capacitances of TX and RX, respectively, satisfying the resonance condition of the power channel

with $\omega_0 = 1/\sqrt{(L_1 C_1)} = 1/\sqrt{(L_2 C_2)}$, where ω_0 is the resonant frequency of the WPT modified in order to include additional decoupling filters that are actually required in the proposed combined system WPT-BLC. These should prevent power from flowing through the PLC modem (to avoid damage) and guarantee optimal coupling between the modem and the WPT system, possibly without affecting the power channel in terms of efficiency. However, with the objective of evaluating the magnetic field distribution through the coils, they are designed and simulated in the frequency domain referring to magnetic field physics. Meanwhile, the electrical components interfaced with these coils are created based on electrical circuit physics. The most widely considered configuration of the WPT system is using two parallel coils with a single TX coil and a single RX coil, [13–15]. In fact, the electrical performances of the proposed design are evaluated as a function of the misalignment scenarios shown in Figure 1.

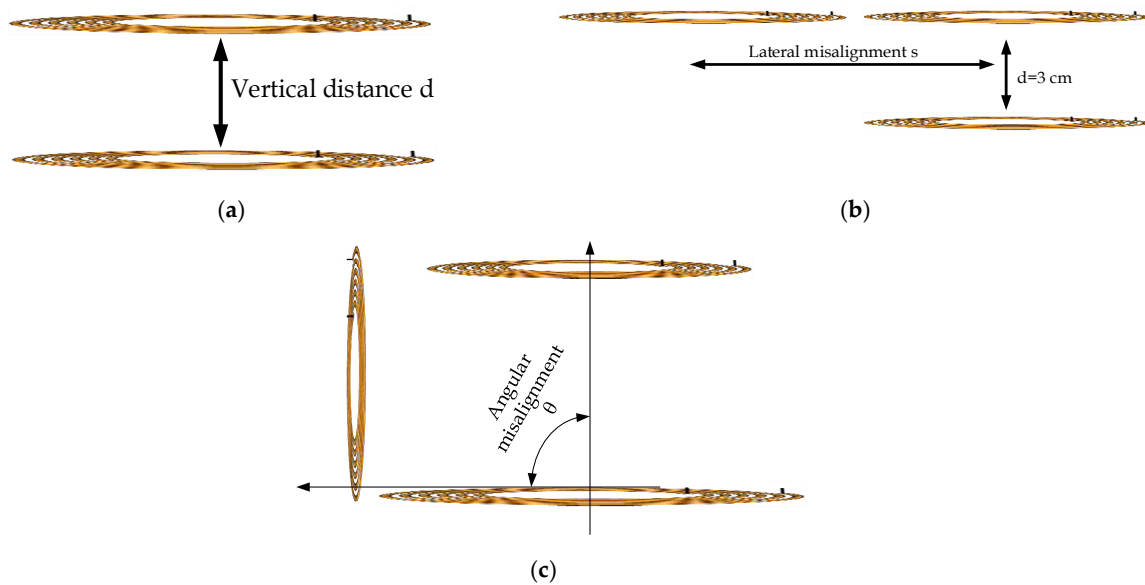


Figure 1. Misalignment scenario top view of Tx and Rx in a study of (a) the coil separation, (b) lateral misalignment, (c) receiver rotating around the transmitter.

The system efficiency highly depends on the magnetic coupling between coils. However, in order to evaluate the mutual inductance M_{12} as a function of the distances, the deviation angle, and the lateral misalignment of the RX-coil, two coils located in the 3D space are considered [13,16], as shown in Figure 2.

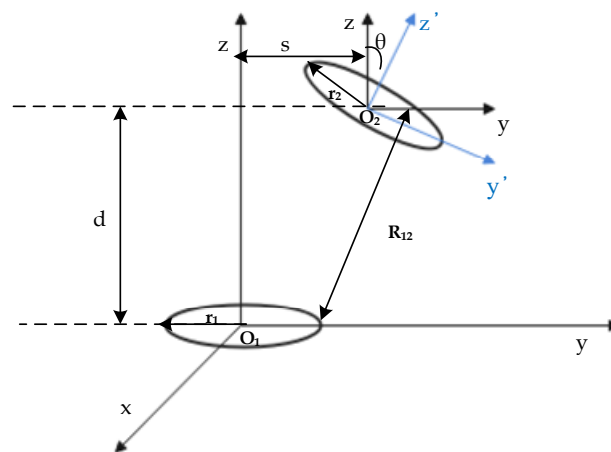


Figure 2. Configuration of the special WPT coils with lateral and angular misalignment.

The mutual inductance calculated based on the Neumann formula [14,15] is given by:

$$M_{12} = \frac{\mu_0 N_1 N_2}{4\pi} \iint \frac{dl_1 dl_2}{R_{12}}, \quad (1)$$

where μ_0 is the magnetic permeability of vacuum, N_1, N_2 represent the coils turns, the radii of the coils are r_1 and r_2 , d is the transmission distance, and the lateral and angular misalignments are represented by s and θ , respectively [13], given by:

$$M_{12}(\theta, d, s) = \frac{\mu_0 N_1 N_2 r_1 r_2}{4\pi} \iint \frac{\sin \alpha \sin \phi \cos \theta + \cos \alpha \cos \phi}{R_{12}} d\alpha d\phi, \quad (2)$$

where the limits of α and ϕ are both $[0, 2\pi]$ and:

$$R_{12} = \left[r_1^2 + r_2^2 + d^2 + s^2 + 2sr_2 \cos \phi \cos \theta - 2sr_1 \cos \alpha 2r_1 r_2 (\cos \alpha \cos \phi \cos \theta + \sin \alpha \sin \phi) - 2r_2 d \cos \phi \sin \theta \right]^{\frac{1}{2}}, \quad (3)$$

The energy efficiency can be written as a function of the mutual inductance M_{12} given by [17–19].

$$\eta_W = \frac{R_L M_{12}^2 \omega^2}{\left((R_L + R_{p2})^2 + X_2 \right) (R_s + R_{p1}) + (R_L + R_{p2}) M_{12}^2 \omega^2}, \quad (4)$$

However, the optimum load for maximum power transfer is determined by maximizing $\frac{\partial P_L}{\partial R_L} = 0$, where the output power of the WPT system is given by [17,19].

$$P_L = R_L I_2^2 = \frac{R_L M_{12}^2 \omega^2 V_s^2}{\left(M_{12}^2 \omega^2 + R_{eq1} R_{p2} + R_{eq1} R_L - X_1 X_2 \right)^2 + \left(R_{eq1} X_2 + R_{p2} X_1 + R_L X_1 \right)^2}, \quad (5)$$

This analysis demonstrates that the maximum power efficiency in the WPT system is achieved at the resonance frequency ($X_i = 0$). However, it is worth noting that the bandwidth of the transfer function of the WPT channel also depends on the load resistance, the distance between coils, the horizontal misalignment, and the deviation angle of the receiving coil.

3. Requirement for Optimal Channel Capacity

The quality factor (Q) represents a critical compromise in designing the shared WPT-PLC channel to accommodate for both power and data signals, $\left(Q = \frac{f}{BW} \right)$ [20–25]. In fact, the designer usually faces the problem of compromising between power efficiency and distortions induced by a high-power WPT link that affects the inductive broadband over power line (BPL) communication channel, which conveys low-power modulated data signals. However, in order to illustrate this concept, the inductive two-coil WPT system with its equivalent circuit is shown in Figure 3a for performing a frequency sweep AC simulation. The two-port S-parameter simulation setup used to characterize the transfer function of the power link, $H_p(f) = V_L(f) V_S(f)$, of the wireless inductive channel is shown in Figure 3b.

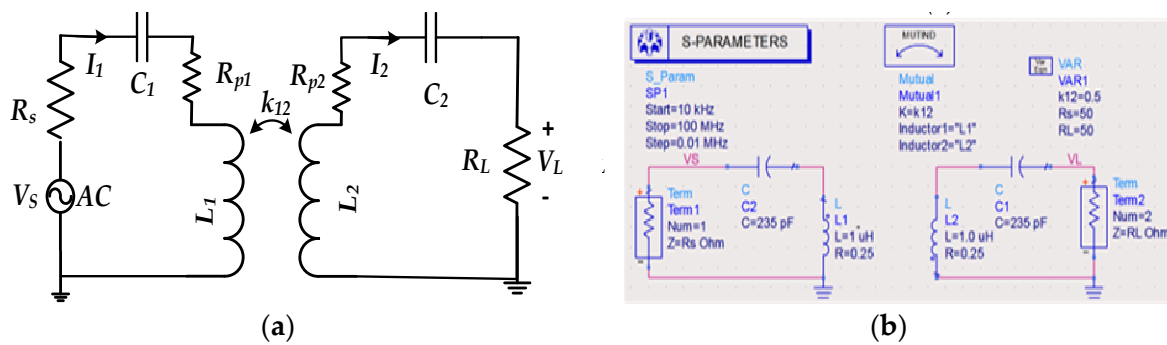


Figure 3. Circuit model of a two-coil WPT system used to characterize the inductively coupled two-coil inductive channel. (a) AC simulation setup. (b) Two-port S-parameter simulation setup.

The simulation results of the power transfer function magnitude, $|H_p(f)|$, and the sidebands of the modulated baseband data signal are added around the data carrier frequency (i.e., $f_c = 65$ MHz), as shown in Figure 4. The HF sidebands of the spectrum of the modulated signal are located aside from the WPT channel bandwidth, leading to high attenuation of the data signal. The bandwidth of the baseband signal should not exceed the half bandwidth of the resonant inductive channel to reduce the distortion and attention of the HF data signal.

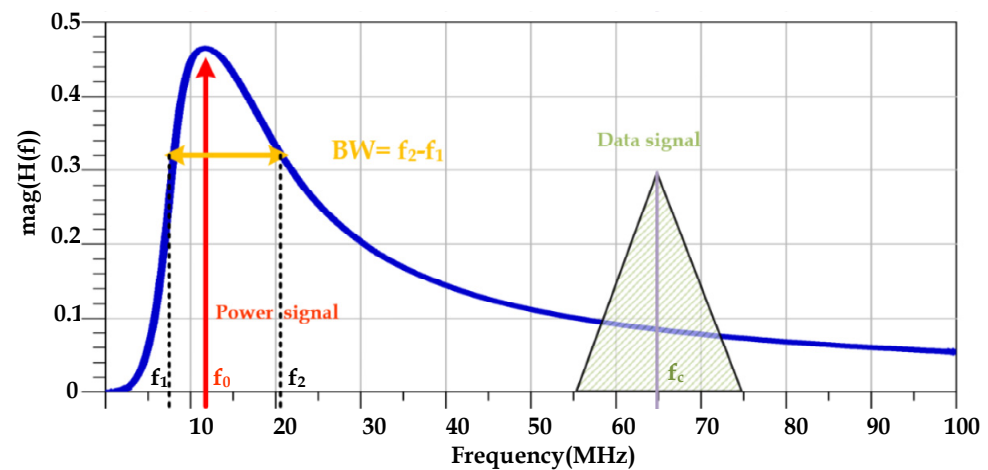


Figure 4. $|H(f)|$ of the resonant inductive (e.g., $f_0 \cong 10$ MHz) of the channel formed by the two-coil system with a coupling factor $k_{12} = 0.5$. The spectrum of the modulated HF data sideband is shown by the data carrier frequency (i.e., $f_c = 65$ MHz) along with baseband signal bandwidth.

For example, let us suppose that $f_c = f_0 = 10$ MHz and high $Q = 50$; therefore, $BW = 200$ kHz. The data rate is approximately equal to 100 kbps when the load modulation is used with an encoded on-off binary signal in the backward communication [24]. However, at a low-quality factor $Q = 5$, the data rate can theoretically achieve 1 Mbps. Unfortunately, this results in low power efficiency. Consequently, Q is the critical trade-off that the designer needs to balance to ensure both efficient power and high data rate communication through the two-coil circuit.

However, the Shannon–Hartley approach is used to calculate the channel capacity metric while considering the same assumptions proposed in previous studies [19]. In fact, the achieved data rate calculated as a function of the different misalignment proposed previously in Figure 3 can be a good approach while evaluating the performance of the proposed systems in handling a high data rate communication speed [21,22], given as:

$$\begin{cases} C = B \log_2(1 + |H_d(f, M, R_L)|^2 SNR) df \\ S(f) = |H_d(f, M, R_L)|^2 S_I \end{cases} \quad (6)$$

where the channel bandwidth $B = [0, 10]$ MHz, and the channel’s transfer functions H_d and H_p are both dependent on the influencing misalignment factors, namely the distance d , the Rx tilt angle θ , and the lateral displacement s of the receiving coil. Considering a resistive load with $R_L = R_s = 50 \Omega$, the achieved data rate is evaluated only as a function of the misalignment scenarios between the transceivers.

4. Simulation Results and Analysis

4.1. Magnetic Field Evaluation Considering Misalignment Scenarios

The magnetic field behavior created by two coils, i.e., planar spiral coils, is studied and an equivalent model composed of a 3D mutually coupled inductor is established based on COMSOL Multiphysics, as shown in Figure 5, and the parameters of the coil are summarized in Table 1.

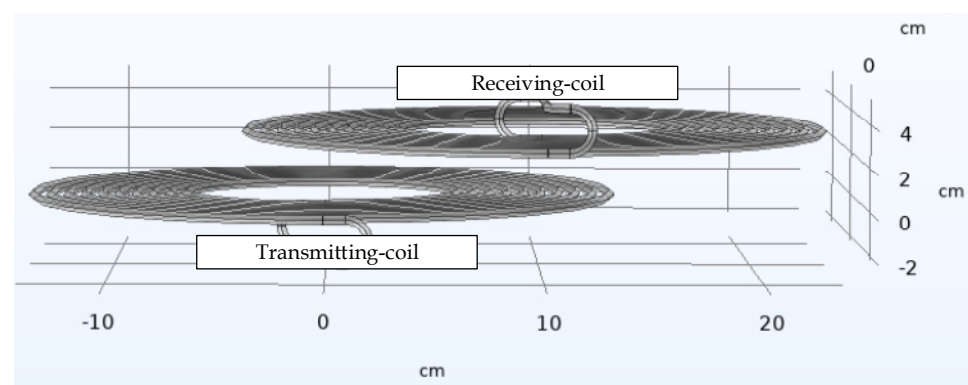


Figure 5. Geometry setup of two-coil system.

Table 1. Parameters of the planar spiral coils.

Parameters	Values
Turns number	10
Cable material	Copper
Cable radius	2 mm
Major radius	5 cm
Radial pitch	7 mm

The frequency domain simulation is also performed and the electric circuit module is added to interface the (RLC) resonant circuit with the AC-DC model with the magnetic field module. The parameters of the electronics components are reported in Table 2.

Table 2. Circuit component and parameter values of the two-coil system simulation setup.

Parameters	Values
f_0	5 MHz
$C_1 = C_2$	45.8 nF
$R_{p1} = R_{p2}$	0.03 Ω
$L_1 = L_2$	17.863 μ H
$R_s = R_L$	50 Ω

In order to achieve a correct signal transmission and reception through the WPT coils system, it is important to characterize the coils, which are the core of the system. The magnetic field distribution is evaluated at the resonance frequency $f_0 = 5$ MHz; meanwhile, the distance between the coils is set to be 4 cm. However, as can be seen in Figure 6a, the highest flux density values occur on the inner ends of the transmitter coil $B_{max} = 0.17$ mT, and the induced field becomes significantly smaller when the distance is equal to the

outer diameter of the coil. Moreover, the magnetic field in dB of the integrated power data links results are shown in Figure 6b, and it is clear that the high-intensity magnetic field is located around the TX coil ranging from -68 dB to -90 dB.

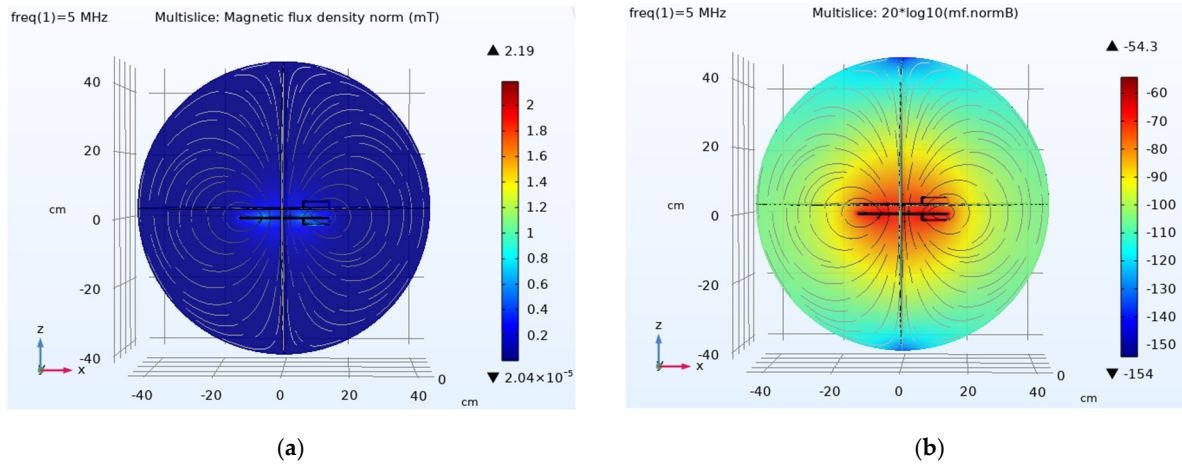


Figure 6. Simulation results at $f_0 = 5$ MHz with $d = 4$ cm; (a) magnetic field distribution; (b) magnetic field in dB.

The B-field of the two-coil system is also evaluated as a function of the lateral and angular misalignment, as shown in Figure 7. However, the module of the magnetic flux density (mT) clearly varies as a function of the deviation angle and the horizontal misalignment. In particular, for an optimum amount of current produced by the transmit coil in the receive coil, the two coils are preferably aligned and ideally oriented such that the receiver coil embedded in the UAVs is perpendicular to the magnetic flux created by the base station transmitter coil (i.e., the axis of the receiver coil is parallel to the magnetic flux) [25].

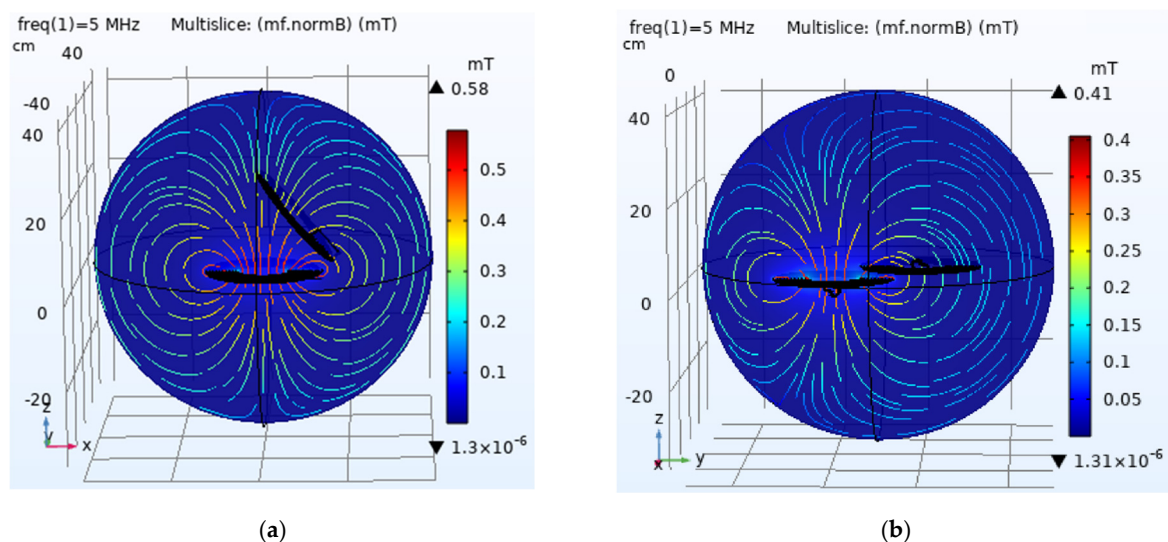


Figure 7. Magnetic field simulation results: (a) angular misalignment; (b) lateral misalignment; $f_0 = 5$ MHz.

Therefore, by using the parametric scanning in COMSOL on the tilt angle of the receiving coil, the horizontal misalignment, and the distance between the transceivers, the mutual inductance M_{12} is dependent on all these parameters, and consequently, the system efficiency and the channel capacity are influenced by the variation of these geometric influencing factors. However, a detailed evaluation of both metrics is performed in the

next subsection wherein the deviation angle of the transmitting coil is fixed and the tuning capacitors are connected in series with the coils keeping the system resonating at 5 MHz.

4.2. Performances of the Data and Power Links of the Two-Coils System

While evaluating the frequency response of the WPT channel in the frequency band [0–10] MHz, the parameters for the components of the equivalent circuit are given, as presented in Table 2, by considering a parametric simulation. The transfer function of the power link (i.e., $|H_p(f)| = |V_L(f)|/|V_s(f)|$) of the two-coil circuit is determined as a function of different misalignment scenarios while considering a fixed resistive load $R_L = 50 \Omega$, as shown in Figure 8.

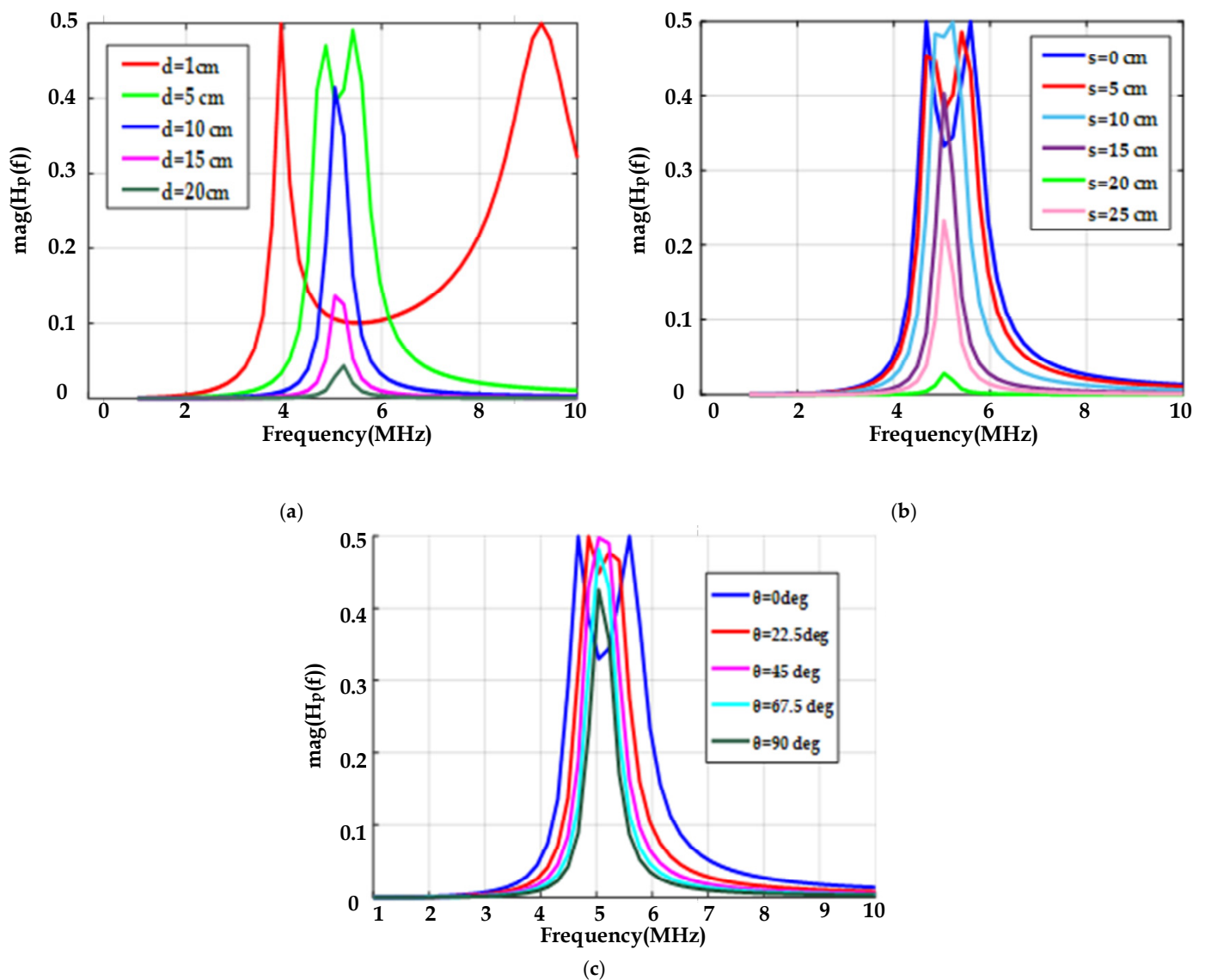


Figure 8. Simulation results power transfer function for $R_s = R_L = 50 \Omega$; (a) distance d between the transceivers; (b) lateral displacement of the RX coil for $d = 5$ cm; (c) angle deviation θ .

This system aims to improve the problem of unsustainable drone life, for autonomous charging, to complete long-term operational requirements. However, by creating a base station equipped with the transmitting coil while the receiving coil is mounted on the drones, in this case, the drones need to reach the available charging station, land automatically and the battery, cognitively, can be recharged. In fact, the electrical performances of the two-coil channel, i.e., the system efficiency, can be studied as a function of each in order to extract the

worst-case misalignment scenario. Firstly, it is clear from Figure 9a that the efficiency drops sharply with the increase in the vertical transfer distance. The effective transfer distance, which is defined as the distance between the fixed transmitting coil and the critical point at which the WPT system performances start decreasing as a function of the distance, can be determined from the graphs with $d_{\text{eff}} = 5$ cm. Secondly, the dependency of the system efficiency on the horizontal misalignment, generally caused by the poor landing precision of UAV, is evaluated and the result is shown in Figure 9b, setting the vertical distance at 3 cm and the deviation angle $\theta = 0$ deg; only the lateral displacement (cm) is considered as variable. Finally, to determine the influences of deviation angle on the system efficiency, the tilt angle of the RX coil varies in the range of 0° to 90° , and the obtained results are shown in Figure 9c. The results show that the PTE highly depends on the deviation angle, and the maximum efficiency ($\eta = 0.9$) is reached with $\theta = 0$ deg.

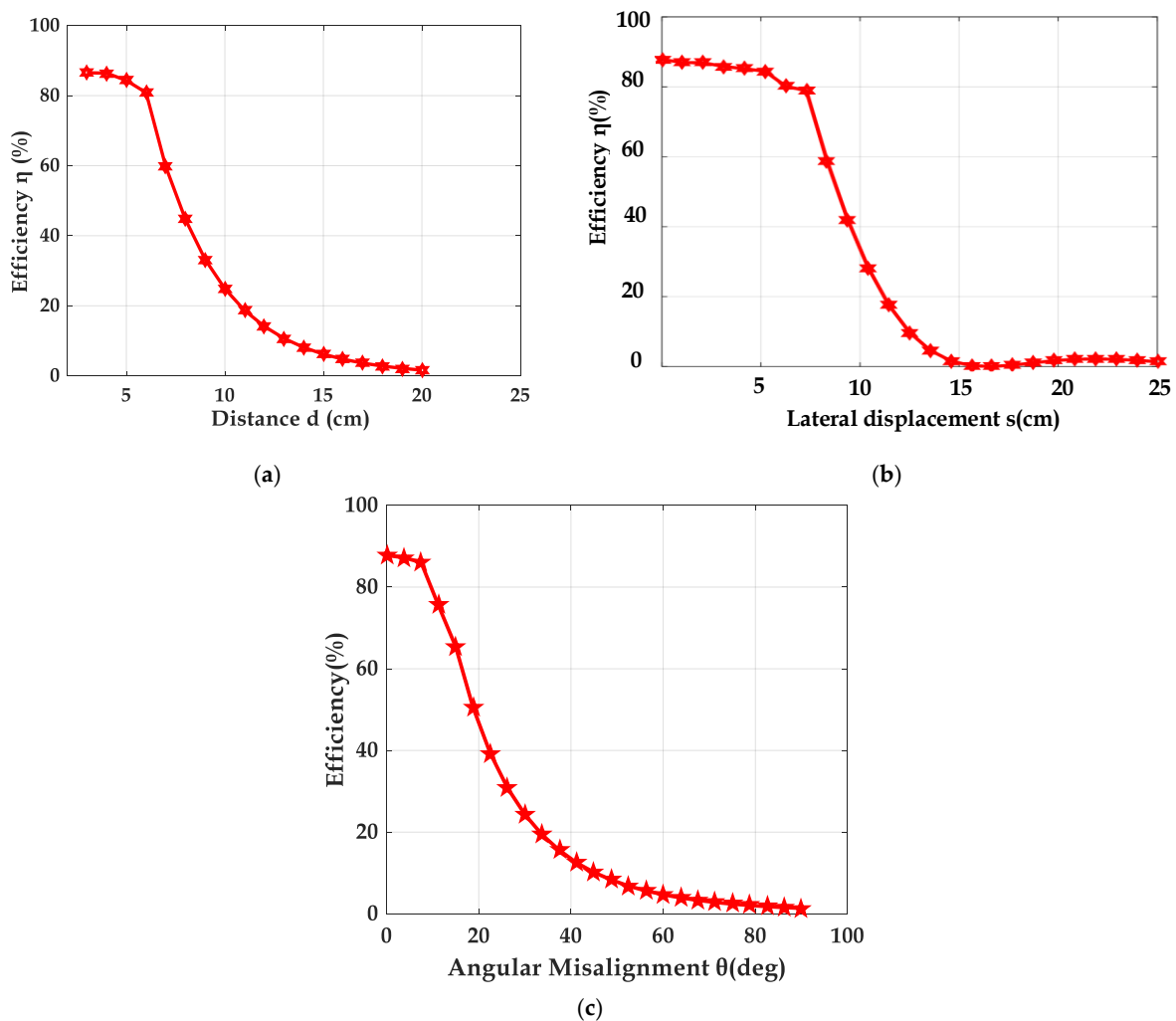


Figure 9. Simulation results of the system efficiency for $R_s = R_L = 50 \Omega$; (a) distance d between the transceivers; (b) lateral displacement of the RX coil for $d = 5$ cm; (c) angle deviation θ .

In order to evaluate the dependency of the system channel capacity on its directional characteristics, the theoretical channel capacity is calculated based on Shannon–Hartley (6) in the frequency band 1 MHz–10 MHz; considering deferent misalignment, the numerical results of this evaluation are reported in Figure 10. In particular, the obtained results show that the obtained data rate is highly influenced by the coils’ misalignment; in fact, the ideal capacity is sharply curved as a function of the distance between the transceivers Figure 10a and as a function of the deviation angle in Figure 10c. Meanwhile, as the distance between coils increases, resulting in low magnetic field coupling, the data rate decreases. Likewise,

the theoretical capacity is influenced by horizontal misalignment where maximum values are reached when the transceivers are perfectly aligned, as shown in Figure 10b. In general, the channel capacity is calculated in a reduced frequency band [1–10] MHz, which can explain the lower value obtained for the data rate. Moreover, the channel capacity is calculated for different SNR values; the obtained result shows that a high data rate is reached under an acceptable and rational noise scenario and for higher SNR values.

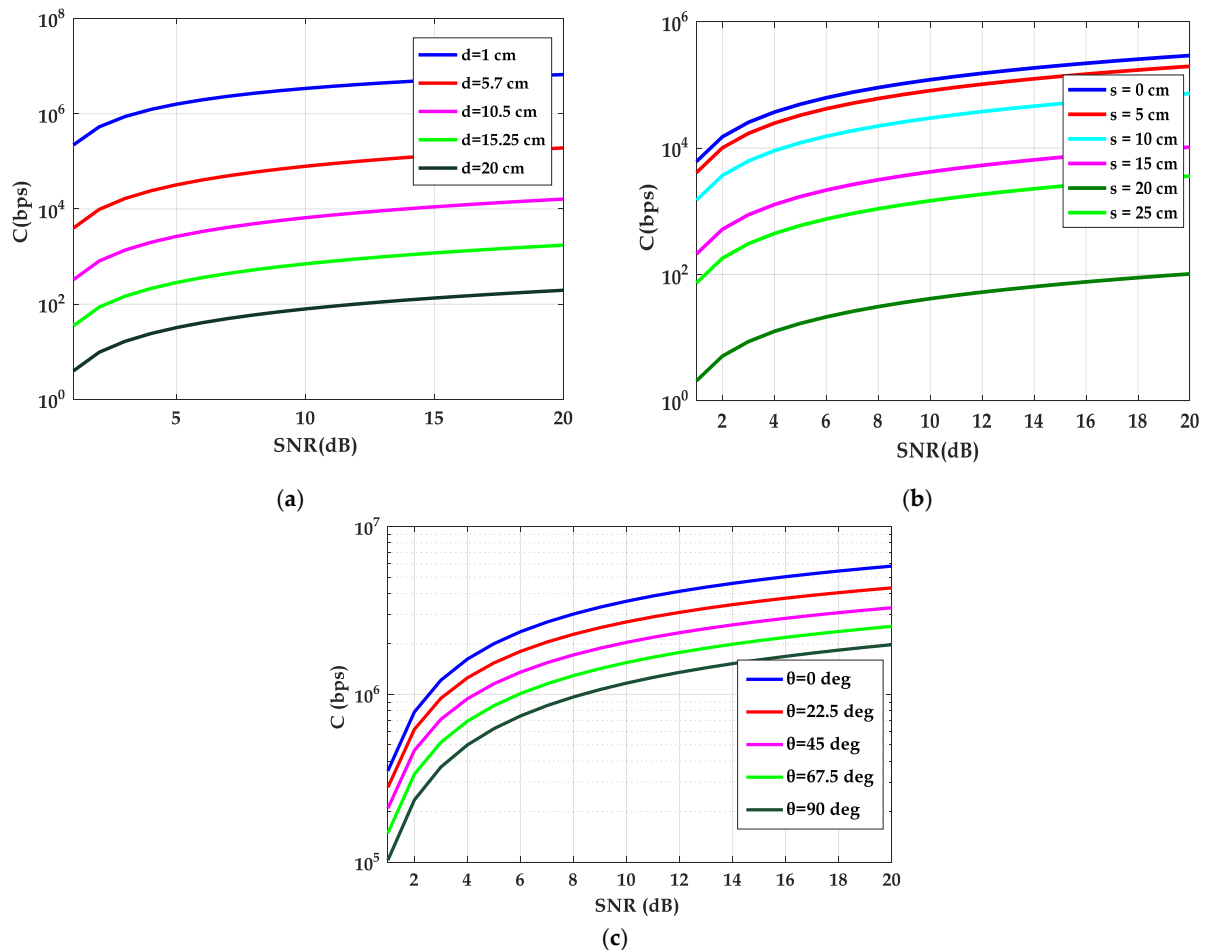


Figure 10. Simulation results of channel capacity for $R_s = R_L = 50 \Omega$; (a) distance d between the transceivers; (b) lateral displacement of the RX coil for $d = 5$ cm; (c) angle deviation θ .

Finally, the worst-case misalignment is extracted from the previous analysis— $d = 20$ cm, $\theta = 90$ deg, and $s = 20$ cm—and evaluated as a function of the SNR values; the results are reported in Table 3.

Table 3. The channel capacity calculated under different misalignment scenarios.

SNR (dB)	C_{\max} ($d = 20$ cm)	C_{\max} ($s = 20$ cm)	C_{\max} ($\theta = 90$ deg)
10 dB	79.547 bps	41.4249 bps	1.16698 bps
15 dB	134.82 bps	70.203 bps	1.606 bps
20 dB	196.005 bps	102.072 bps	1.977 bps

5. Experimental Measurements

The theoretical analysis results previously presented can be experimentally verified based on the setup shown in Figure 11, which is composed of a frequency generator, transmitting and receiving coils, with two resonance capacitances in order to ensure the resonance capacitance, and, finally, a variable resistive load.

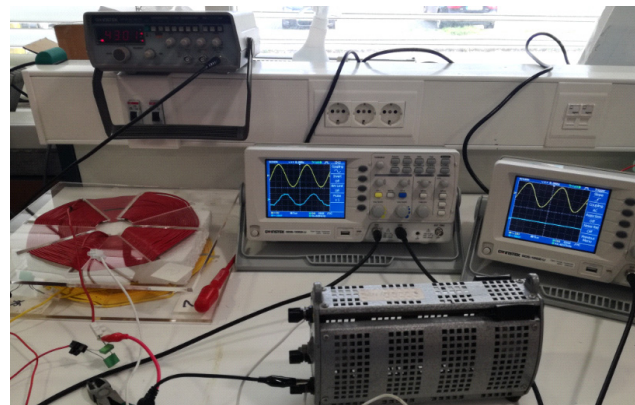


Figure 11. Experimental setup used to characterize the resonant inductive coupling.

The WPT resonant frequency is set to 150 kHz as a good agreement between efficiency and low electronic complexity. The results of the transmission distance are experimentally verified and the graphs of the relationship between transmission distance and mutual inductance are shown in Figure 12a while that between transmission distance and the frequency is also represented in Figure 12b.

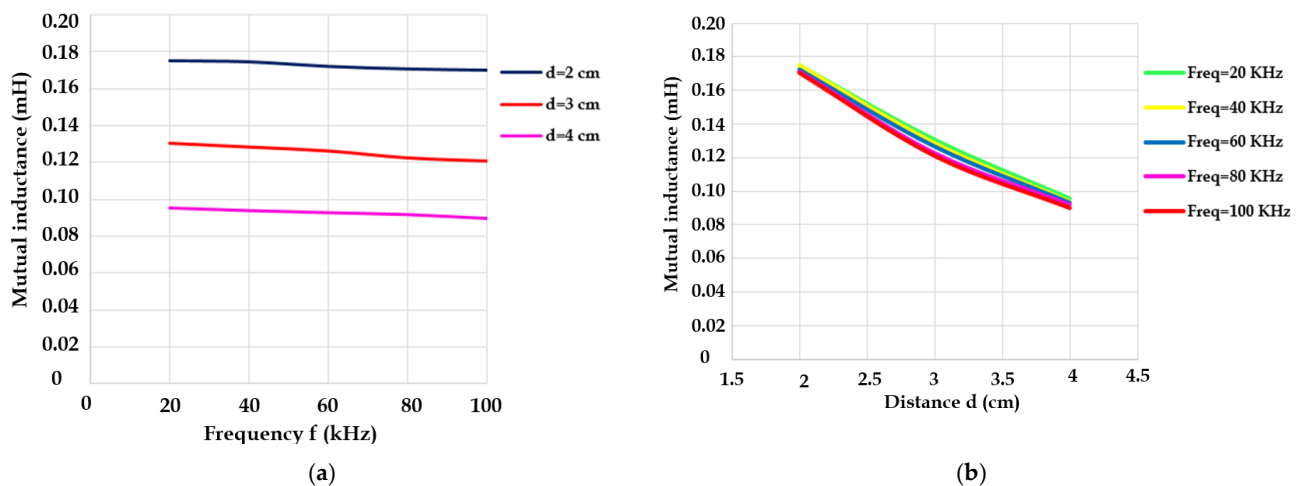


Figure 12. Mutual inductance variation as function of (a) frequency and (b) distance.

It is worth noting that the mutual inductance M_{12} highly depends on the distance between the transmitting and receiving coils as shown in Figure 12a, for instance, the calculated mutual inductance M_{12} reached 0.18 uH for a reduced distance ($d = 2$ cm) between the coils however as this distance increases, meanwhile reducing the magnetic coupling coefficient, while it slightly decreases as a function of the kHz frequency range e.g., freq $\in [20, 100]$ kHz.

Moreover, the maximum received power P_{out} and the system efficiency η are calculated as a function of load resistance R_L , and the numerical results of this evaluation are reported in Figure 13. The maximum received power and efficiency are achieved at the resonance for $R_L \cong 3.3 \Omega$. However, it is worth noting that, as the R_L exceeds 17.5 Ω , the received power slightly decreases while the efficiency highly decreases with a faster slope, which means that efficiency of such inductive coupling system highly influenced by the output load. Also, it is noticeable that good values of the transmitted power are achieved for $R_L \in [3.3, 17.5] \Omega$, for instance, $P_{out} \in [34, 27.5]$ w for $R_L \in [3.3, 17.5] \Omega$.

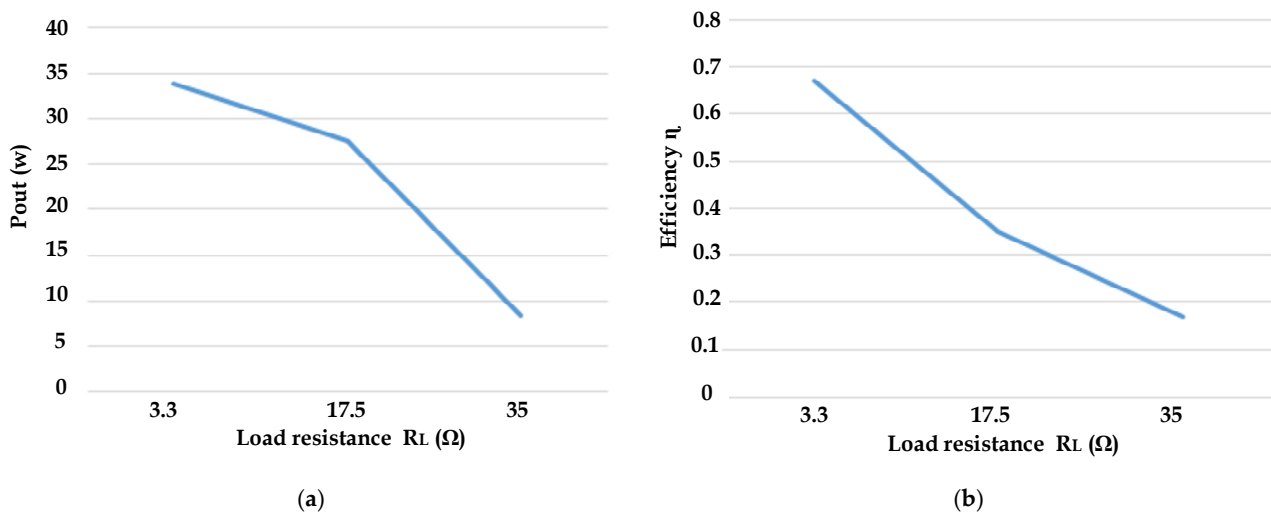


Figure 13. (a) Maximum received power P_{out} (b) the system efficiency η variation as a function of load.

6. Conclusions

The investigation presented in this paper was directed toward pushing WPT technology to the next level. The proposed design explores the effective integration of the data and power signals in order to share the same inductive channel. The influence of system directional characteristics was performed by considering a symmetrical WPT system achieving a theoretical data rate from tens of bit/s to a few Mbit/s. However, maximum efficiency was reached while reducing the misalignment of the receiving coil.

Geometrical requirements must be considered by choosing a smaller RX coil, which can increase tolerance to coil misalignment.

Author Contributions: Conceptualization, S.Z., W.D., L.R., R.M. and H.B.; Methodology, S.Z. and W.D.; Software, S.Z.; Validation, S.Z., W.D., L.R., R.M. and H.B.; Formal Analysis, S.Z.; Investigation, S.Z.; Writing—Original Draft Preparation, S.Z.; Writing—Review and Editing, S.Z., W.D., R.M. and H.B.; Visualization, S.Z.; Supervision, W.D., R.M. and H.B. All authors have read and agreed to the published version of the manuscript.

Funding: This research received no external funding.

Acknowledgments: Acknowledgment to the Ministry of Higher Education and Scientific Research, Republic of Tunisia; by FCT through IDMEC, under LAETA, project UIDB/50022/2020; by FCT through ICT (Institute of Earth Sciences) project, project UIDB/04683/2020.

Conflicts of Interest: The authors declare no conflict of interest.

References

- Li, B.; Fei, Z.; Zhang, Y. UAV Communications for 5G and beyond: Recent advances and future trends. *IEEE Internet Things J.* **2019**, *6*, 2241–2263. [CrossRef]
- Batista, N.C.; Melicio, R.; Santos, L.F. Large geographical area aerial surveillance systems data network infrastructure managed by artificial intelligence and certified over blockchain: A review. *Networks* **2021**, *1*, 335–353. [CrossRef]
- Yang, G.; Lin, X.; Li, Y.; Cui, H.; Xu, M.; Wu, D.; Rydén, H.; Redhwan, S.B. A Telecom Perspective on the Internet of Drones: From LTE-advanced to 5G. Networking and Internet Architecture. Available online: <https://arxiv.org/abs/1803.11048> (accessed on 15 January 2022).
- Merkert, R.; Bushell, J. Managing the drone revolution: A systematic literature review into the current use of airborne drones and future strategic directions for their effective control. *J. Air Transp. Manag.* **2020**, *89*, 101929. [CrossRef] [PubMed]
- Campi, T.; Dionisi, F.; Cruciani, S.; De Santis, V. Magnetic field levels in drones equipped with wireless power transfer technology. In Proceedings of the IEEE 2016 Asia-Pacific International Symposium on Electromagnetic Compatibility (APEMC), Shenzhen, China, 17–21 May 2016; pp. 544–547.
- Campi, T.; Cruciani, S.; Feliziani, M. Wireless power transfer technology applied to an autonomous electric UAV with a small secondary coil. *Energies* **2018**, *11*, 352. [CrossRef]

7. Polo, J.; Hontecillas, L.; Izquierdo, I.; Casas, O. Micro air vehicles energy transportation for a wireless power transfer system. *Int. J. Micro Air Veh.* **2019**, *11*, 1–13. [[CrossRef](#)]
8. Simic, M.; Bil, C.; Vojisavljevic, V. Investigation in wireless power transmission for UAV charging. *Procedia Comput. Sci.* **2015**, *60*, 1846–1855. [[CrossRef](#)]
9. Lu, M.; Bagheri, M.; James, A.P.; Phung, T. Wireless charging techniques for UAVs: A review, reconceptualization, and extension. *IEEE Access* **2018**, *6*, 29865–29884. [[CrossRef](#)]
10. Baikova, H.N.; Valtchev, S.S.; Melicio, R.; Pires, V.M. Wireless power transfer impact on data channel. In Proceedings of the IEEE International Symposium on Power Electronics, Electrical Drives and Motion (SPEEDAM 2016), Capri, Italy, 22–24 June 2016; pp. 582–587.
11. Romba, L.F.; Valtchev, S.S.; Melicio, R. Three-phase magnetic field tested in wireless power transfer system. *Int. Rev. Electr. Eng.* **2016**, *11*, 586–597. [[CrossRef](#)]
12. Barmada, S.; Dionigi, M.; Mezzanotte, P.; Tucci, M. Design and experimental characterization of a combined WPT–PLC system. In *Wireless Power Transfer*; Cambridge University Press: Cambridge, UK, 2017; pp. 160–170.
13. Huang, W.; Ku, H. Analysis and optimization of wireless power transfer efficiency considering the tilt angle of a coil. *J. Electromagn. Eng. Sci.* **2018**, *18*, 13–19. [[CrossRef](#)]
14. Li, Y.; Liu, J.; Yang, Q.; Ni, X.; Zhai, Y.; Lou, Z. Directional characteristics of wireless power transfer via coupled magnetic resonance. *Electronics* **2020**, *9*, 1910. [[CrossRef](#)]
15. Wang, W.; Wang, H.; Li, Q.; Xu, J.; Meng, T.; Zhang, B.; Zhang, Z. Analysis and compensation of incomplete coupling for omnidirectional wireless power transfer. *Energies* **2019**, *12*, 3277. [[CrossRef](#)]
16. Li, Y.; Jiang, S.; Liu, X.L.; Li, Q.; Dong, W.H.; Liu, J.M.; Ni, X. Influences of coil radius on effective transfer distance in WPT system. *IEEE Access* **2019**, *7*, 125960–125968. [[CrossRef](#)]
17. Czarnecki, A.E. Efficient Inductively Coupled Resonant Power Transfer for an Implantable Electroencephalography Recording Device. Master’s Thesis, Northeastern University, Boston, MA, USA, 2012.
18. Johnson, E. Resonant Wireless Power Transfer with Embedded Communication for More Versatile and Efficient Applications. Master’s Thesis, Massachusetts Institute of Technology, Cambridge, MA, USA, 2016.
19. Islam, A.B. Design of Wireless Power Transfer and Data Telemetry System for Biomedical Applications. Ph.D. Thesis, University of Tennessee, Knoxville, TN, USA, 2011.
20. Barmada, S.; Raugi, M.; Tucci, M.; Mezzanotte, P.; Dionigi, M. Combining WPT and PLC: A review. In Proceedings of the IEEE 2nd International Forum on Research and Technologies for Society and Industry Leveraging a Better Tomorrow (RTSI), Bologna, Italy, 7–9 September 2016; pp. 1–4.
21. Zouaoui, S.; Souilem, M.; Dghais, W.; Radwan, A.; Barmada, S.; Tucci, M. Wireless power transfer and data communication cognitive radio through two-coil inductive channel. In Proceedings of the IEEE Global Communications Conference (GLOBECOM), Waikoloa, HI, USA, 9–13 December 2019; pp. 1–6.
22. Zouaoui, S.; Dghais, W.; Melicio, R.; Belgacem, H. Omnidirectional WPT and data communication for electric air vehicles: Feasibility study. *Energies* **2020**, *13*, 6480. [[CrossRef](#)]
23. Barmada, S.; Tucci, M.; Fontana, N.; Dghais, W.; Raugi, M. Design and realization of a multiple access wireless power transfer system for optimal power line communication data transfer. *Energies* **2019**, *12*, 988. [[CrossRef](#)]
24. Wu, J.; Zhao, C.; Lin, Z.; Du, J.; Hu, Y.; He, X. Wireless power and data transfer via a common inductive link using frequency division multiplexing. *IEEE Trans. Ind. Electron.* **2015**, *62*, 7810–7820. [[CrossRef](#)]
25. Baikova, E.N.; Valtchev, S.S.; Melicio, R.; Krusteva, A.; Gigov, G. Study on electromagnetic emissions from wireless energy transfer. In Proceedings of the IEEE 17th International Conference on Power Electronics and Motion Control (PEMC 2016), Varna, Bulgaria, 25–30 September 2016; pp. 492–497.